Optimal Load Frequency Control for Interconnected Power Systems using Optimized PI-PD Controller with TCSC and HVDC Integration

Vivek Nath[1], D.K Sambariya[2]
[1]Department of Electrical Engineering, Rajasthan Technical University, Kota, India
[2]Department of Electrical Engineering, Rajasthan Technical University, Kota, India

Article Info	ABSTRACT
	The aim of this study is to develop a consistent load frequency control system for a multi-area power system (PS) network that uses a variety of energy sources. The research focuses on improving frequency regulation and ensuring stability in the face of uncertainties and disturbances. This article introduces load frequency control (LFC) analysis for multi-area multi-source (MAMS) interconnected power systems (IPS). Each area comprises thermal reheat turbines, a hydro unit, and gas turbines as generating units. The effect of AVR after TCSC and HVDC is extensively investigated in this research article. The suggested hybrid PI-PD controller is tuned using the PSO optimization technique, presenting a novel and efficient approach to addressing the complexities of multi-area power systems. Another significant advancement is the incorporation of high-voltage direct current (HVDC) and thyristor-controlled series compensator (TCSC) as auxiliary parameters. This dual integration improves system robustness by managing power flow variations and enhancing transient response, ultimately contributing to the overall stability of the multi-area power grid. Four different power system models are studied. To determine the best value for controllers, all four performance metrics are employed to define the optimal parameters of the PI-PD and PID controller. Eigenvalues analysis is also conducted to find the stability of the MAMS power system. The robustness of the proposed PI-PD controller at different loading conditions is tested, and the superiority of the suggested controller is determined by executing it in four different cases. A step-load of 10% is applied for each area. Non-linearities such as governor dead band (GDB), governor rate constraints (GRC), and the boiler are also included in the MAMS-IPS. Based on settling-time (ST) and rise-time (RT), the performance of the proposed controller is compared with various PID controllers optimized with novel evolutionary algorithms from recent published literature. MATLAB 2018@ software is used for simulation purposes.

Corresponding Author:

Vivek Nath
Department of Electrical Engineering,
Rajasthan Technical University, RTU, kota
Rajasthan Technical University, Rawathbhata Road Kota-324010. RTU, Rajastha, India
Email: Viveknath311989@gmail.com

1. INTRODUCTION

Modern power systems require efficient and robust control strategies to preserve stability and dependability in the face of dynamic operational problems. In an interconnected power system, maintaining voltage and frequency within desirable limits is a crucial task. The imbalance between reactive and active power flow is caused by random variations in load as demand changes. Active power is related to frequency variation, and for constant active-power flow, frequency should be controlled. Voltage fluctuation depends on

reactive power. For the reliable operation of the interlinked power system (IPS), two control loops are implemented one is the load frequency control (LFC) Loop and the automatic voltage regulator AVR Control Loop [1]. The speed governor action in the LFC control loop can significantly reduce frequency deviation. Furthermore, by controlling the excitation of the synchronous generator, reactive power of the system can be regulated. Incorporating the AVR loop with the LFC loop minimizes voltage fluctuation through reactive power control [2, 3].

Secondary controllers are required to efficiently minimize frequency, voltage variation, and tie-line power fluctuation [4]. This research investigates Load Frequency Control (LFC) utilizing a novel approach - the Multi-Area Multi-Source Interlinked Power System (MAMS-IPS) coupled with Automatic Voltage Regulator (AVR). The inquiry progresses through the examination of four separate power system models, each of which provides dynamic insights into the system's behavior.The design and tuning of controller parameters for optimal performance are crucial. In this presented work, a naturally inspired algorithm (PSO) is applied for tuning conventional PID and hybride PI-PD controller parameters.

Through literature survey, it is evident that many researchers have shown interest in the conventional PID/PI controller, utilizing it as a secondary controller for LFC. In this literature, PID controller parameters are tuned using the PSO algorithm and the results are compared with genetic algorithm and hill climbing optimization techniques as illustrated in [5]. GA-PID acts as a secondary controller to minimize the automatic control error (ACE) Error, using a thermal source, and the results are compared with the PI/PID conventional controller as given in [6]. PID parameters tuned by DE optimization for LFC are illustrated in [7], where thermal hydro and gas are used as generating units. The hybrid bacterial foreign optimization algorithm is used for optimizing PID parameters, with thermal-PV hybrid sources as generating units as given in [8]. TCSC-SMES is used to mitigate the deviation of responses of LFC as given in [9]. This literature also includes DE-based fuzzy PID as a secondary controller and the implementation of TCSC with AC tie line for making the power system stable as illustrated in [4, 10]. Intelligent controllers such as a Fuzzy controller, NARMA-L2 controller based on ANN technique, and Adaptive Fuzzy logic controller are proposed in this literature [11-15]. To mitigate Tie-Line Power Transfer capability, HVDC lines are incorporated parallel with AC lines as illustrated in [16-18].The goals of this article is described below

- The main contribution of this work is to provide a robust controller for the LFC-AVR control loop (MAMS-IPS) that incorporates nonlinearities such as governor rate constraints (GRC) and governor dead band (GDB). A boiler block is also utilized with the reheat turbine.
- High Voltage Direct Current (HVDC) lines are combined with AC tie-line (LFC-AVR-HVDC) to minimize tie-line power deviation.
- A thyristor control series capacitor TCSC controller is fitted beside the HVDC to improve the power flow stability of the IPS.
- The PI-PD controller has been implemented, and its parameters have been tuned using the PSO. The performance of PSO-PID is also evaluated for the LFC-AVR power system model. The effectiveness of hybrid PI-PD is justified over conventional PID controllers.
- Finding eigenvalues for a closed-loop MAMS-IPS is also carried out for stability analysis.
- The efficiency and rigidity of the proposed controller are tested for various loading conditions.

In this literature, MAMS-IPS incorporated with TCSC is considered for LFC study, and the effect of non-linearity and Automatic Voltage Regulation (AVR) is not taken into consideration with MAMS-IPS [19-21]. The effect of nonlinearities such as GRC and GDB, as well as AVR and HVDC links with AC-link, is taken into account in this presented article. The effect of AVR is not explored in this research, and no eigenvalue analysis is executed to determine the stability of the suggested model in this literature [10, 22-25]. AVR is used in both areas of the presented article, and eigenvalue analysis is also conducted on all four cases to ensure the system's stability. Robustness is also assessed under different loading conditions. This article also considers the effect of a boiler with a reheat turbine. In this literature, MAMS-IPS with AVR is considered for LFC research. However, the effects of fact devices and non-linearity constraints are not taken into account. Eigenvalue analysis for the proposed power system (PS) model is also not performed in this published work [22, 26-27]. Non-linearity and the effect of the Fact-Device (TCSC) are measured in this presented work, and eigenvalue analysis and robustness testing at various loading conditions are performed.

2. SYSTEM DESCRIPTION
The suggested simulation model consists of three types of generating units reheat thermal unit with boiler block incorporated with it, hydro, and gas unit. These two areas having three generating units in each

area are interconnected Through Tie-Line. PID and PI-PD controllers are implemented to minimize the (ACE) Error. ACE is equivalent to sum of $\Delta f_i . B_i$, ΔP_i. For making the system more effective for power generation and Transmission AVR is connected in each area for controlling the Voltage Fluctuation. MAMS-IPS incorporated with AVR is demonstrated in Figure 1. T_{gr}, T_{rt} and T_t are the Time-constant of Thermal power plants. K_{re} is the gain of Thermal-units. T_{gh}, T_{rh} and T_w are the Time-constant of the hydro unit. B and C are gas turbine Time-constant. X and Y are the lead-lag Time constant of the Governor. The combustion reaction Time constant is Represented By T_{cr} and T_f is the Fuel Time-constant. Compressor Discharge volume Time-constant in (sec) is denoted by T_{CD}. A load of 10% (0.01 P.U) is given to each area. Matlab/Simulink Environment is used for Transfer-Function (TF) model Development. Data for the MAMS-IPS Transfer Function Model is given in Appendix. Controllers (PID/PI-PD) parameters are optimized using the PSO algorithm.

The Automatic Voltage regulator (AVR) is an essential module of a power system, which let the voltage of an alternator to be maintained at a constant value. The AVR model is demonstrated in Figure 2, which comprises coupling coefficients. AVR system has a sensor unit having K_s a gain-parameter and T_s a Time constant in (sec). The amplifier Block consists of K_A a gain and T_A a Time constant. Exciter a single order Transfer-Function (TF) has K_E as a gain and T_E as a Time constant. Field of generator consists of K_G a gain and T_G a time constant. V_{ref} is a step response given as a Reference for the AVR system.

The Transfer Function (TF) equation for Thermal Reheat Turbine is given below in equation (1)

$$G_T(s) = \frac{(1+s\,T_{re}\,K_{re})}{(1+s\,T_{gre})(1+s\,T_{re})(1+s\,T_{tr})} \tag{1}$$

The Transfer Function (TF) equation for Hydro Turbine is given below by equation (2)

$$G_H(s) = \frac{(1+sT_{rs})(1-sT_w)}{(1+s\,T_h)(1+s\,T_{rh})(1+0.5\,T_{ws})} \tag{2}$$

The equation for Gas Turbine in form of (TF) is given below in equation (3)

$$G_G(s) = \frac{(1+xs)(1-T_{CR}\,s)a}{(1+ys)(c+bs)(1+T_F\,s)(1+T_{CD}\,s)} \tag{3}$$
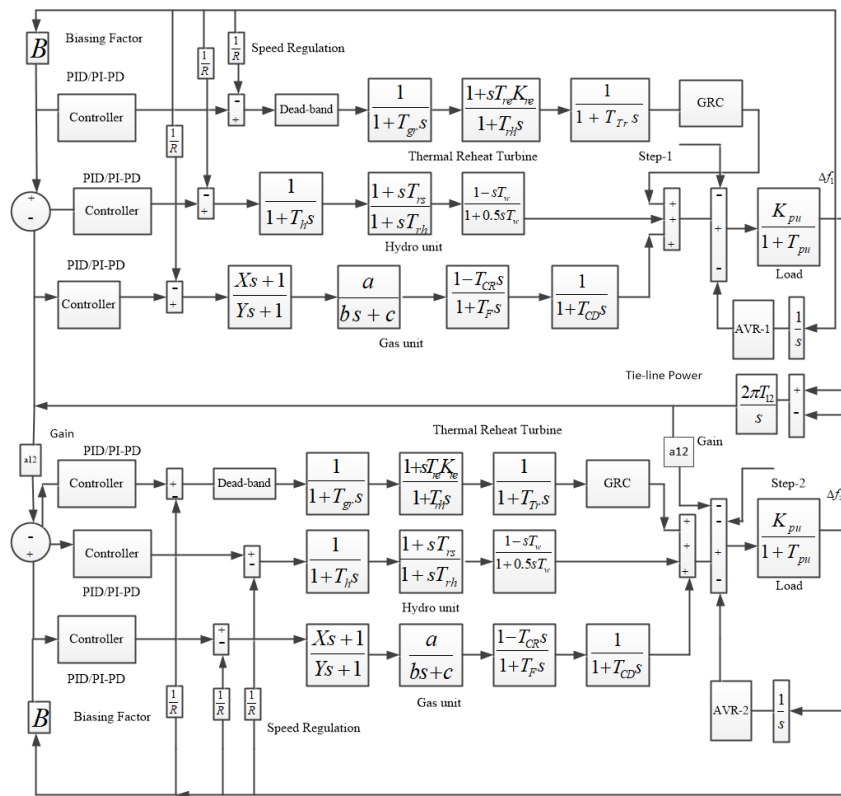
Figure 1. Mathematical Transfer-Function (TF) model of MAMS-IPS

The load side transfer function is modeled approximately as given by equation (4)

$$G_p(s) = \frac{K_{ps}}{1+sT_{ps}} \tag{4}$$

Where $K_{ps} = \frac{1}{D}$ and $T_{ps} = \frac{2H}{fD}$

The deviation in Tie-Line power deviation ($\Delta P_{1,2}$) can be stated as shown in equation (5)

$$\Delta P_{tie1,2} = T_{12}(\Delta\delta_1 - \Delta\delta_2) \tag{5}$$

Frequency deviation (Δf) in the power system is proportional to the variation in phase angle, which is expressed by equation (6) and equation (7)

$$\Delta\delta_1 = 2\Pi \int \Delta f_1 . dt \tag{6}$$

$$\Delta\delta_2 = 2\Pi \int \Delta f_2 . dt \tag{7}$$

Tie-Line power flow is expressed by equation (8)

$$\Delta P_{tie1,2} = 2\Pi T_{12} \int^{\int} (\Delta f_1 - \Delta f_2). dt \tag{8}$$

By applying Laplace Transformation above equation is given by equation (9)

$$\Delta P_{tie1,2} = \frac{|v_1|v_2||}{x_{12}} sin(\delta_1 - \delta_2) \tag{9}$$

By using equation (10) to equation (11) and equation (12) can be written as

$$\Delta P_{tie1,2} = T_{12}(\Delta\delta_1 - \Delta\delta_2) \tag{10}$$

$$T_{12} = \frac{|v_1||v_2|}{x_{12}} cos(\delta_1 - \delta_2) \tag{11}$$

Where T_{12} is synchronizing power coefficient, then

$$\Delta P_{tie1,2}(s) = \frac{2\Pi T_{12}}{s} (\Delta f_1(s) - \Delta f_2(s)) \tag{12}$$

The AVR effect on the MAMS power plant is also considered For the LFC study. The mathematical model of AVR is provided below in Figure 2. With its Transfer-Function equation (13-16)
The transfer function equation for the Amplifier is given below in equation (13)

$$G_A(s) = \frac{K_A}{1+sT_A} \tag{13}$$

The transfer function equation for Exciter is given below in equation (14)

$$G_E(s) = \frac{K_E}{1+sT_E} \tag{14}$$

The transfer function equation for Sensor is provided below by equation (15)

$$G_s(s) = \frac{K_s}{1+sT_s} \tag{15}$$

The transfer function equation for Generator is provided below in equation (16)

$$G_G(s) = \frac{K_s}{1+sT_G} \tag{16}$$
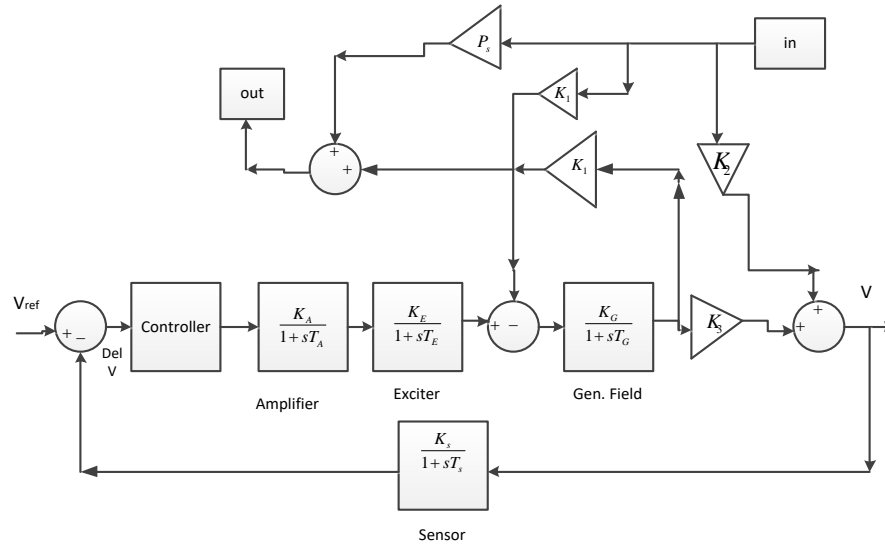
Figure 2. Automatic Voltage Regulator (AVR) Transfer Function Model

2.1 Interconnected Power System Nonlinearities
2.1.1. Governor Rate Constraints (GRC)

The term GRC, known as Governor Rate Constraint, is imposed by power system operators to maintain the grid's steadiness and consistency. This constraint ensures a controlled and consistent shift in the output of a generator. As defined by [2, 28], GRC is expressed as the generator's rated capacity per minute. A GRC limit of 10% per minute indicates that the generator can change its rated output by up to 10% of its capacity in one minute. The internal structure of governor rate constraints is depicted in Figure 3
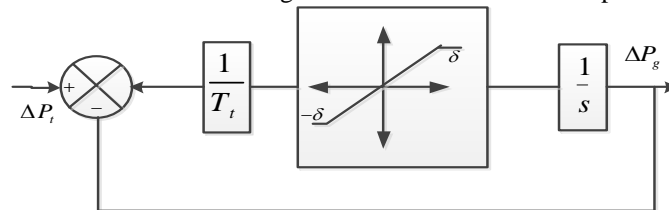
Figure 3. Block Diagram of Governor Rate Constraints

2.1.2. Governor Dead Band (GDB)

As the input to the governor is increased, the speed of the governor also increases proportionally. However, due to the dead band, the governor does not react immediately; it responds when a particular limit set with the help of the Governor Dead Band (GDB) is reached. The entire magnitude of the continued speed varies within a certain range proposed by the operator, and the valve position remains constant. The application of the Dead Band increases the apparent speed regulation value [2, 29]. If the power output crosses a particular limit but is within the GDB range, no corrective action is taken by the governor at that time. However, if the power output changes beyond that limit (GDB range), the governor's control action takes place until the system returns to normal conditions. The block diagram of the Dead Band for MAMS-IPS is illustrated in Figure 4.
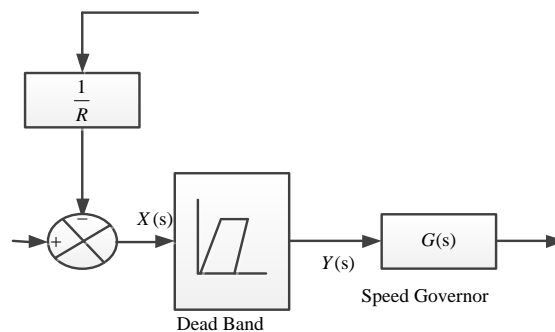
Figure 4. Block Diagram of Dead Band for IPS

2.1.3. Boiler

The turbine control valve plays a crucial role in controlling power generation. Proper combustion rate control is essential for regulating the output of the boiler. The drum-type boiler is illustrated in Figure 5. It's noteworthy that coal-fired units exhibit a slower response compared to gas and oil-fired boiler systems. This model can study oil or gas-fired services with insufficient combustion control, as well as coal-fired plants with highly-tuned ignition control. In thermal power plants, turbine control valves are commonly employed to initiate changes in power generation [30]. Essential control measures are promptly executed after a change in pressure and steam drift rate is sensed by the boiler, as emphasized in [2, 31].
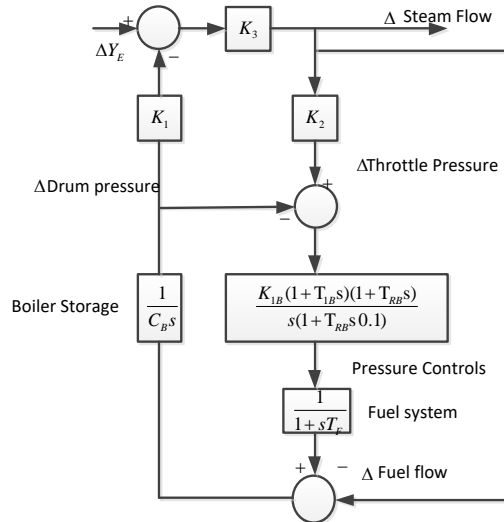
Figure 5. Boiler Dynamics Transfer Function Model

2.2. TCSC modeling in LFC

The capacity of a transmission line can be controlled by varying the reactance of the line. The implementation of Thyristor-Controlled Series Capacitor (TCSC) allows for the adjustment of both inductive and capacitive reactance of the line by varying the firing angles. TCSC is constructed by linking the Thyristor Controlled Reactor (TCR) in parallel with the capacitor [4]. Through the insertion of capacitive reactance with the help of TCSC, the overall reactance of the line is reduced, leading to an increase in the transmission capacity of the line. With TCSC, both the reactive and active power flow of the line can be regulated [3]. This helps mitigate frequency variation and improves the flow of real power through the tie-line [19].

The flow of current is modeled and expressed by equation (17), flow of current is between area-1 and area-2.

$$I_{12} = \frac{|v_1|\angle(\delta_1) - |v_2|\angle(\delta_2)}{j(x_{12} - x_{TCSC})} \tag{17}$$

X_{12} is Tie-Line reactance
X_{TCSC} is TCSC reactance

$$\Delta\delta_1 = 2\Pi \int \Delta f_1. dt \tag{18}$$

$$\Delta\delta_2 = 2\Pi \int \Delta f_2. dt \tag{19}$$

The Linearized model of TCSC is modeled and expressed by equation (20)

$$\Delta k_{PC}(s) = \frac{K_{TCSC}}{1+sT_{TCSC}}\Delta E(s) \tag{20}$$

K_{TCSC} = Gain of TCSC constant
T_{TCSC} = The time constant of TCSC
TCSC controller is equipped close to area-1 in the Transmission -Line, Δf_1 which is taken as an error. $\Delta E(s)$ is an error signal, $\Delta K_{pc}(s)$ output signal

2.3. Conventional HVDC Linearized Model

A single line layout of a two-area power system is demonstrated in Figure 6, For controlling DC-Line power flow, Inverter and rectifier are incorporated with DC-line work as switching devices. Power Flow through AC and DC Tie-Line is given as $\Delta P_{tie1,2ac}$ and $\Delta P_{tie1,2dc}$ respectively. Detail theory of HVDC for LFC is given in [17, 18, 36]. DC-Line First order transfer function is given by equation (21).

$$\Delta P_{tie,dc} = \frac{K_{DC}}{1+sT_{DC}} \tag{21}$$

K_{DC} Indicates HVDC model Gain,T_{DC} Time constant of HVDC line.
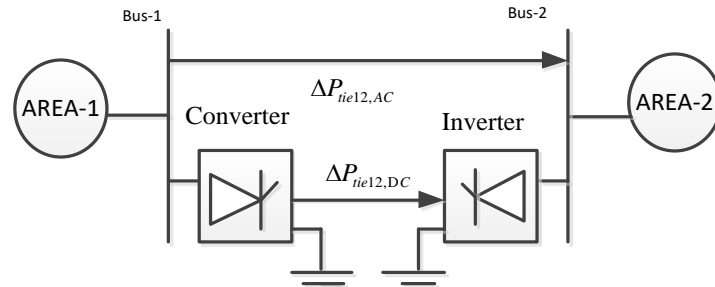
Figure 6. HVDC Connections with AC Tie-Line

The exact HVDC Link Transfer Function is given in Figure 7, which is implemented in MAMS-IPS.
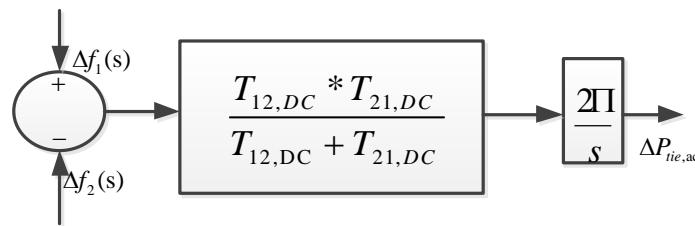
Figure 7. Proposed a transfer Function model for HVDC

T_{12} and T_{21} are equivalent synchronizing factors of the HVDC Link. Detail Modelling of the HVDC Transfer Function (TF) For LFC is Demonstrated in this reference [37].

3.   PROPOSED METHODOLOGY FOR MAMS-IPS

A PID controller is a conventional controller. Because of its simplicity and effectiveness, it is widely used in industrial applications [32]. The PID controller can be modified to enhance its performance. In this article, the PID controller is implemented to minimize the steady-state error (SSE) of the voltage variation. PID control is further modified for the PI-PD controller; its results are quite better than those of the PID controller. PI-PD and PID controller gains are maximized using the PSO technique [33, 34]. Figure 8 demonstrates the proposed controller scheme with MAMS-IPS. The PI-PD controller transfer function model is summarized below, and its input is given by equation (22).

$$U(s) = (K_{p1} + \frac{K_i}{s}) E(s) - (K_{p2} + K_d s) Y(s) \tag{22}$$

$U(s)$ and $E(s)$ are control and Error signals, Correspondingly given by equation (23)

$$E(s) = Y(s) - R(s) \tag{23}$$

E (S) is the error signal, R (S) is a reference signal, and Y (S) is an output signal.
Optimization of cost Function (J) is used to determine the tuned variables of the PID/PI-PD controller using the suggested PSO optimization technique. For optimizing the error signal, various objective indices are taken into consideration, such as integral square error (ISE), integral time absolute error (ITAE), integral

absolute error (IAE), and integral time square error (ITSE) [35]. The proposed mechanism for MAMS-IPS is demonstrated in Figure 8.
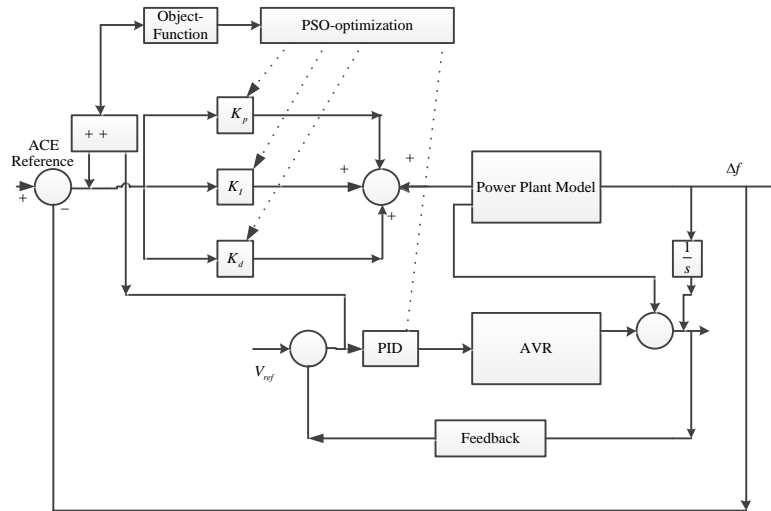
Figure 8. Suggested Controller scheme For MAMS-IPS [34]

$$J_{ISE} = \int_0^T (\Delta f_1^2 + \Delta f_2^2 + \Delta v_{t1}^2 + \Delta v_{t2}^2 + \Delta P_{tie12}^2). \, dt \tag{24}$$

$$J_{IAE} = \int_0^{T\int} (|\Delta f_1| + |\Delta f_2| + |\Delta v_{t1}| + |\Delta v_{t2}| + |\Delta P_{tie12}|). \, dt \tag{25}$$

$$J_{ITAE} = \int_0^{T\int} t.(|\Delta f_1| + |\Delta f_2| + |\Delta v_{t1}| + |\Delta v_{t2}| + |\Delta P_{tie12}|). \, dt \tag{26}$$

$$J_{ITSE} = \int_0^{T\int} t.(\Delta f_1^2 + \Delta f_2^2 + \Delta v_{t1}^2 + \Delta v_{t2}^2 + \Delta P_{tie12}^2). \, dt \tag{27}$$

Performance Indices from equation (24-27) are used for finding optimized parameters.

4. PARTICLE SWARM OPTIMIZATION (PSO) TECHNIQUE

Kennedy and Eberhart in 1995 developed a novel computational method known as the particle swarm optimization (PSO) technique. This optimization procedure is encouraged by observing the behavior of bird and fish congregations. It is an evolutionary method that fits the groundwork of swarm intelligence. Every particle in the swarm represents a potential solution. particle position is updated by knowledge gained from its own experience and knowledge collected by the swarm's behavior [5, 38]. The best solution is obtained by the particle adjusting its position cooperatively. The steps used by the PSO algorithm for finding the best solution are as follows:

1. Initialization: a population of particles is initialized with their position and velocities in the search space.
2. Evaluation: objectives or fitness for every particle are evaluated based on its position.
3. Personal Best Update: Each particle's current fitness is compared with its prior best fitness value, which is known as its personal best. Updating the best position and fitness is done if present fitness is better.
4. Global Best Update: The best fitness of the entire population has been discovered, and it is regarded as the greatest in the world. Update the global best position accordingly.
5. Velocities and Position Updation: Based on its existing velocity, personal best position, and global best position, every particle's velocities and positions are modernized by considering inertia (W), cognitive components, and social components.
6. Termination condition: stop if a satisfactory solution is reached; if not, go back to step 2.

For a wide range of optimization problems, PSO is successfully applied. It is helpful for continuous, discrete, and multi-objective optimizations. PSO is a sophisticated optimization method that mimics the

working performance of social organisms [39, 40]. The increment in position and velocity of the particle is given by equations (28) and (29).

$$x_i(t+1) = x_i(t) + v_i(t+1) \tag{28}$$

$$v_i(t+1) = wv_i(t) + c_1(P_i(t) - x_i(t)) + c_2(g(t) - x_i(t)) \tag{29}$$

$$v_{ij}(t+1) = wv_{ij}(t) + r_1 c_1(P_{ij}(t) - x_{ij}(t)) + r_2 c_2(g_{ij}(t) - x_{ij}(t)) \tag{30}$$

$$x_{ij}(t+1) = x_{ij}(t) + v_{ij}(t+1) \tag{31}$$

$$W = \frac{Max_{iteration} - I_{iteration}}{Max_{iteration}} \tag{32}$$

Where v_i and x_i are the Velocity and position of a particle at the ith position, j is the dimension. C_1 and C_2 are the acceleration coefficient. r_1 and r_2 are the casual number their range lies between 0 and 1. w represents the inertia weight factor. $Max_{iteration}$ shows the maximum number of iterations and $I_{teration}$ represents the current value of iterations. $c_1(P_i(t) - x_i(t))$ Represents cognitive elements, $c_2(g(t) - x_i(t))$ represents social elements. equation (30) and equation (31) show an increment in the position and velocity of a particle in two dimensions. Examining mechanism of the PSO technique is shown in Figure 9.
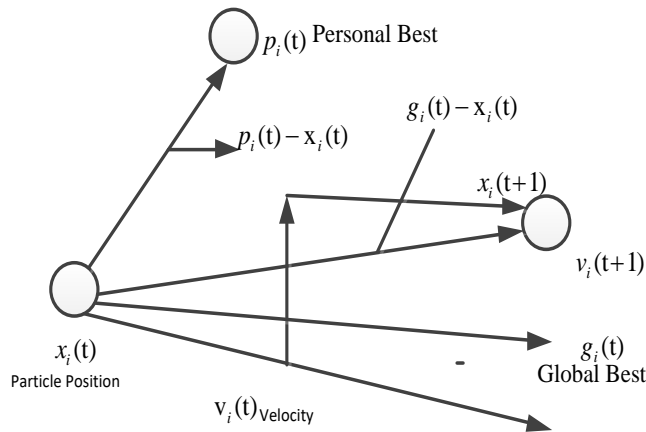
Figure 9. Searching mechanism of the PSO algorithm

The parameters of the proposed PID controller obtained by the PSO optimization Technique are given in Table 1. Internal structure of the PI-PD controller is demonstrated in Figure.10 .Parameters of the Proposed PD-PI controller obtained by applying the PSO optimization Technique is illustrated in Table 2.

Table 1. Parameters of Proposed PID-PSO for all Four Cases (MAMS-IPS)

S.no	Proposed controller PID	LFC-Area-1	LFC-Area-2	AVR-Area-1	AVR-area-2
	Case-01 proposed-PID controller FOR LFC-AVR				
1	K_p	-1.73276021	-1.2004517	0.662117993	1.92744388
2	K_I	0.7869079993	-0.08745199	0.505108298	1.18482684
3	K_d	-0.493114608	0.412367221	0.0880071642	1.7151654
	Case-02 proposed-PID controller FOR LFC-AVR-HVDC				
1	K_p	0.4496782899	-1.846888053	1.98669918	0.769568522
2	K_I	0.2798267015	0.4290195944	0.959787982	0.3538425345
3	K_d	0.6991956778	-0.180243327	1.19632686	0.0683659813
	Case-03 proposed-PID controller FOR LFC-AVR-TCSC				
1	K_p	-0.05637752	0.399382430	0.1840253840	1.98537112
2	K_I	0.2338735746	0.2116283034	0.46448301670	-0.28908
3	K_d	-0.010530766	-1.99898889	0.61579579112	-0.594107335
	Case-04 proposed-PID controller FOR LFC-AVR-TCSC-HVDC				
1	K_p	0.9143982	1.10960286	0.319400174	1.47113748
2	K_I	0.4303404	0.60282231	1.1300236796	-0.5208737
3	K_d	0.91612965	-1.69839270	1.99396479	0.089554056

Table 2.Parameter of Proposed PI-PD controller for all four cases (MAMS-IPS)

S.no	Proposed controller PI-PD	LFC-Area-1	LFC-Area-2	AVR-Area-1	AVR-area-2
Case-01 proposed-PI-PD controller FOR LFC-AVR					
1	K_{p1}	0.740535162	-1.998068817	0.404405449	0.0826649867
2	K_I	0.547614848	0.0881993424	0.9990835472	1.378795823
3	K_{p2}	0.223557959	-1.99964966	0.7405585463	1.28520439
4	K_d	0.055657340	-0.098153555	0.2898910858	0.17012322
Case-02 proposed-PI-PD controller FOR LFC-AVR-HVDC					
1	K_{p1}	1.9407089	-1.881890	1.9998578455	0.694878842
2	K_I	0.966342808	0.69436183	0.71403747781	0.412228491
3	K_{p2}	1.63970903	0.3582572895	0.161186122	0.0957256999
4	K_d	0.005091804	-0.101715	0.632939400	0.149213433
Case-03 proposed-PI-PD controller FOR LFC-AVR-TCSC					
1	K_{p1}	-0.69346866	-0.1027585	0.07808292528	0.554745628
2	K_I	1.653451537	0.139224123	1.133577930	1.31883718
3	K_{p2}	-1.58729887	-0.1101788	1.088492665	0.8914935742
4	K_d	-0.67616320	0.221590085	0.1638603042	0.4076887929
Case-04 proposed-PI-PD controller FOR LFC-AVR-TCSC-HVDC					
1	K_{p1}	1.2978969	1.999669281	-3.31594855	1.688250070
2	K_I	1.34904579	1.182468282	0.1801774670	1.58640779
3	K_{p2}	1.222586625	1.196063265	1.14298161	0.7115377056
4	K_d	-0.23677367	1.883073098	0.1007080523	0.7083164540
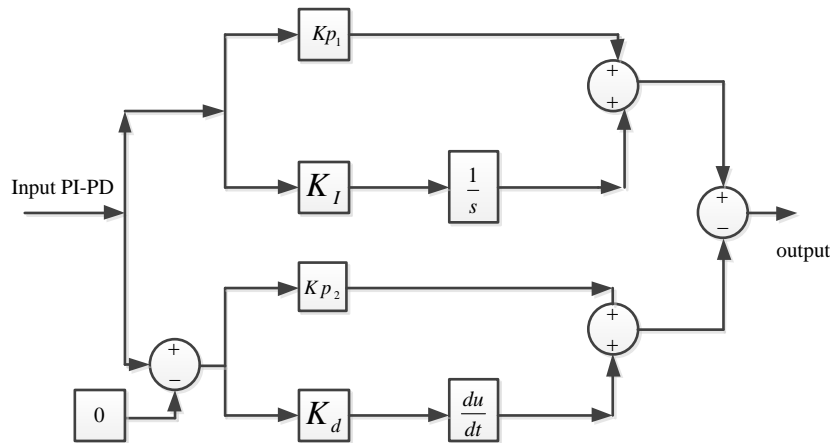
Figure 10. PI-PD controller for MAMS-IPS

5.   RESULT DISCUSSION

The suggested control scheme Validation is done by applying it to MAMS-IPS with nonlinearities such as GBD, GRC, and boiler. The investigation is further extended by applying the suggested controller PID/PI-PD optimized with the help of the PSO Optimization Technique to MAMS-IPS incorporated with AVR. MAMS-IPS is studied by considering four different cases. In the first case, the LFC-AVR model is considered. In the case of no second, LFC-AVR-HVDC is taken into consideration for the load frequency control studied. Case-03 LFC-AVR is incorporated with Fact device (TCSC) to see the effect of TCSC on active power and frequency deviation. In Case-04, LFC-AVR-HVDC-TCSC is taken into consideration for studying the combined effects of DC-Link and Fact Device. The efficiency of the suggested PI-PD and PID controllers is tested for all the different cases. Based on objective functions such as ITAE, IAE, ISE, and ITSE, all four cases' results are compared with each other. Figures 11 to 13 show the output responses, such as change in frequency and tie-line power variation comparison, of all four cases with each other. A PI-PD-optimized controller is used to minimize steady-state error. Figures 14-15 demonstrate the voltage deviation of all the different cases incorporated with the PSO-PI-PD controller. The LFC-AVR-HVDC-TCSC result is superior as compared to other case results. By seeing the responses of frequency and voltage variation, it is apparent that the steady-state error (SSE) of all responses is minimized to near zero by implementing the suggested controller. A comparison of all different cases based on settling time and peak time is given in Tables 3 and 4. MAMS-IPS, having both Fact devices and HVDC, shows better results. The implementation of the suggested PSO-PI-PD controller shows improvement in the output response based on settling time, particularly in frequency and tie-

line power responses. Case-04 demonstrates a notable 68.96% improvement in output responses. Similarly, for Case-04, there is a 60.39% improvement and a significant 78.81% improvement compared to Case-01. The voltage response achieved in Case-04 is well improved, showing a 73.88% enhancement for and a 52.29% improvement for compared to Case-01. Furthermore, the comparison based on performance indices is done. All results are obtained by applying the suggested PSO-PI-PD controller. In Table 5, all performance indicators results are concluded for all different cases. The performance indices, namely ITAE, ITSE, IAE, and ISE, obtained in Case-04 show a significant reduction compared to Case-01. The suggested PI-PD controller in Case-04 achieves a substantial 69.85% reduction in the ITAE objective function, a similarly notable 68.45% reduction in ITSE, a 49.41% reduction in IAE, and a 50.04% reduction in ISE.

The study is further extended by applying a PSO-PID-optimized controller in all different cases to minimize the deviation of the output responses of PS. Figures 16–18 show the comparison of the frequency and tie-line power response of all different cases obtained by implementing a PSO-PID-optimized controller for each area. The Figures 19 and 20 show the voltage responses of both areas. From this comparison, it is also evident that the LFC-AVR incorporates facts and the HVDC gives better results as compared to other cases. Table 6 and Table 7 demonstrate the evaluation of all the different cases based on settling time and peak time. All these results were found with the help of a PSO-PID-optimized controller. Table 8 shows the comparison of all the cases based on performance Indices such as ITAE, IAE, ISE, and ITSE. By absorbing Table 6 and Table 8, it is concluded that the PSO-PI-PD proposed optimized controller gives a better result as compared to the proposed PSO-PID controller. Based on performance indices, it is concluded that by implementing the FACT devices and HVDC with AC-line, the effectiveness of MAMS-IPS with AVR is improved to a great extent.

For analyzing the effect of load change on MAMS-IPS case-04, this is taken into consideration. PSO-PI-PD controller is implemented in both areas to maintain the variation in the frequency and power responses up to an acceptable limit, which is almost near zero. LFC-AVR-TCSC-HVDC power system model is tested at different loading conditions. The efficiency of the recommended controller is not affected by load variations. 10% load variation in both areas at each time is done. The step load is increased, but the steady-state error of the responses remains near zero, so this shows that the suggested PI-PD controller is capable of handling the load variation. Figures 21–23 show the output responses of PS at different step loads. Figures 24 and 25 show the voltage variation of the AVR closed loop. The Figures 26 and 27 show the frequency response, and Figure 28 shows the tie-line power response. Figures 29 and 30 give the voltage responses of both areas; the proposed controller's superiority is seen by comparing its results with recent published literature. Table 9 demonstrates the result comparison of the suggested PI-PD controller based on settling time with recently published literature. The result obtained by the PSO-PI-PD controller is compared with a recently published literature controller based on settling time (ST). It is found that there is a very promising improvement in settling time for the percentage improvement in settling time is 63.93%, 71.11%, and 81.74%, respectively. Additionally, for voltage responses such as and, the percentage improvement is reported as 64.59% and 59.63%. Table 10 shows a comparison based on rise time. The proposed controller result is quite better as compared to the literature-based controller tuned to different evolutionary algorithms. Figure 31 shows the iteration graph obtained by applying the PSO optimization technique to find the optimized value of the suggested PI-PD controller. Figure 32 shows the graph of the number of iterations obtained by the PSO algorithm for tuning the PID controller's parameters for all different cases. Table 11 illustrates the stability analysis based on eigenvalues. This PSO-PI-PD controller is considered for all different cases. By seeing eigenvalues, it is easy to see that the system under study is steady, as all eigenvalues lie on the left half of the s-plane.

Appendix
f =50 Hz;
$B_1 = B_2 = B = 0.45$ MW/Hz;
$P_R = 2000$MW (rating),$P_L = 1740$ MW (small-loading);
$R_1 = R_2 = R_3 = 2.4$Hz/p.u MW;
$pf_{11} = pf_{21} = 0.49666$;
$pf_{12} = pf_{22} = 0.37814$;
$pf_{13} = p_{23} = 0.1522$;
T_{pu} =11.49;
K_{pu} =68.9566 Hz/p.u;
$T_{12} = 0.0433$;
$a_{12} = -1$.

Thermal: $T_{gr} = T_{gr} = T_{gr} = 0.08$ sec; $T_{re1} = T_{re2} = T_{re} = 10$ sec; $K_{r1} = K_{r2} = K_r = 0.30, T_{tr} = T_{tr} = 0.3$ sec.

Hydro: $T_{h1} = T_{h2} = T_h = 28.75, T_{rs1} = T_{rs2} = T_{rs} = 5$ sec; $T_{rh1} = T_{rh2} = T_{rh} = 0.2$ sec; $T_{w1} = T_{w2} = T_w = 1$ sec.

Gas: $b_1 = b_2 = b = 0.5$ sec; $c_1 = c_2 = c = 1$ sec; $X_1 = X_2 = X = 0.6$ sec; $Y_1 = Y_2 = Y = 1$ sec; $T_{cr1} = T_{cr2} = T_{cr} = 0.03$ sec; $T_{f1} = T_{f2} = T_f = 0.23$ sec; $T_{cd1} = T_{cd2} = T_{cd} = 0.2$ sec

AVR models parameters .The time and gain constants of the amplifier are $K_A = 10, T_A = 0.1$ sec, the exciter time constant $K_E = 1, T_E = 0.4$ sec, the generator time constant $K_G = 0.8, T_G = 1.4$, gain and time constant of the sensor $K_s = 1, T_s = 0.05$ sec, $P_s = 1.5$, $K_1 = 0.2, K_2 = -0.2, K_3 = 0.5, K_4 = 1.4$. HVDC unit: $K_{dc} = 1$, $T_{dc} = 0.8$

Parameters used to optimize the PI-PD controller using PSO optimization method for different cases. **For LFC-AVR model which is case-01**, $c_1 = 1.5, c_2 = 2 \, wmax_{min}, n_{pop} = 100, iter_{max} = 100$ $Rmax_{min}, Best\_cos t = 5.3401$. **For Case-02 (LFC-AVR-HVDC)** $Best\_cos t = 4.321101$ **For Case-03(LFC-AVR-TCSC)** $Best\_cos t = 2.8671$ **For case-04 (LFC-AVR-TCSC-HVDC)** $Best\_cos t = 2.21401$

Case-01 = LFC-AVR , Case-02 = LFC-AVR-HVDC, Case-03 = LFC-AVR-TCSC, Case-04 = LFC-AVR-HVDC-TCSC. The case-04 shows superiorty over all cases when obtained responses of these cases are compared with other cases on bases of different constraints,
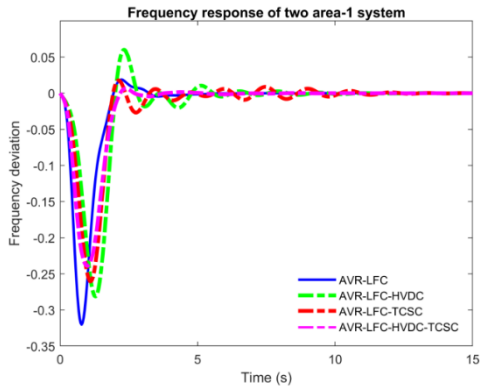
Figure 11. Frequency Deviation of area-1 For MAMS-IPC, PSO-PI-PD all four cases are considered
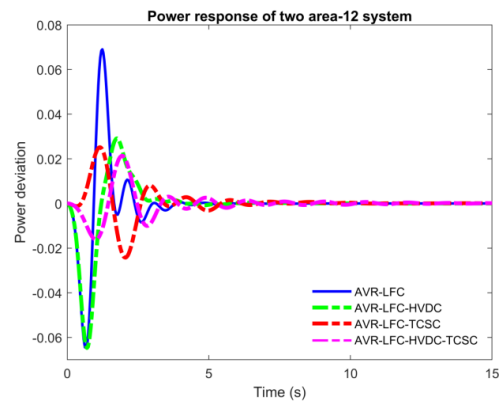
Figure 13. Power Deviation of area-12 For MAMS-IPC, PSO-PI-PD all four cases are considered
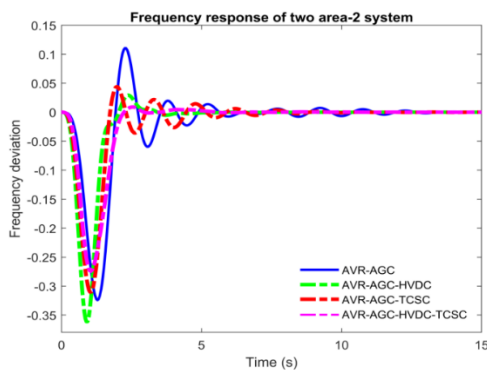
Figure 12. Frequency Deviation of area-2 For MAMS-IPC, PSO-PI-PD all four cases are considered
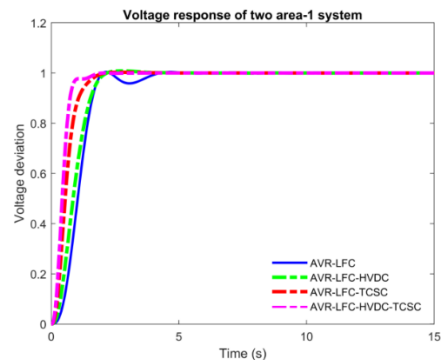
Figure 14. Voltage Deviation of area-1 For MAMS-IPC, PSO-PI-PD all four cases are considered
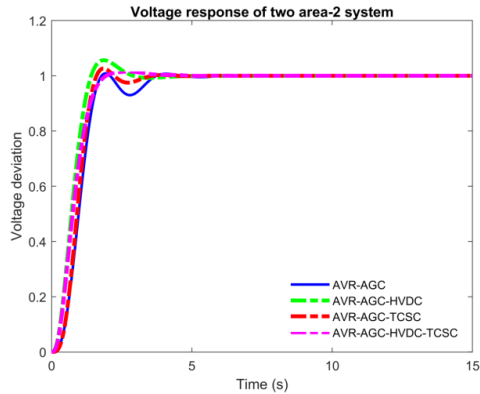
Figure 15.Voltage Deviation of area-2 For MAMS-IPC, PSO-PI-PD all four cases are considered
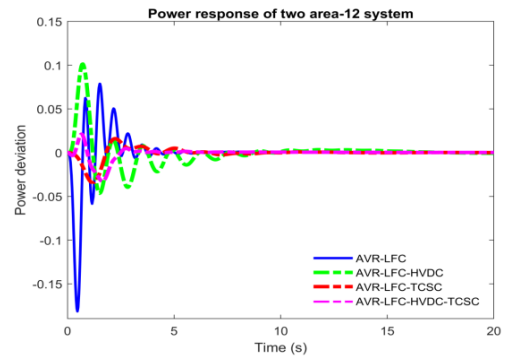
Figure 18. Power Deviation of area-1,2 For MAMS-IPC, PSO-PID all four cases are considered
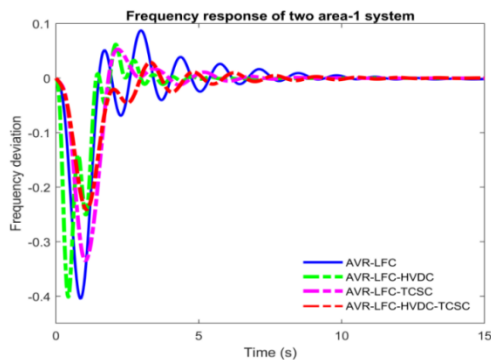
Figure 16. Frequency Deviation of area-1 For MAMS-IPC, PSO-PID all four cases are considered
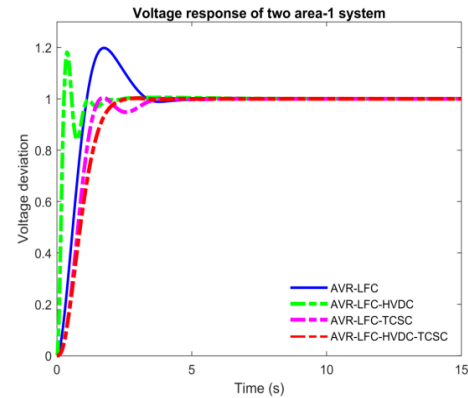
Figure 19. Voltage Deviation of area-1 For MAMS-IPC, PSO-PID all four cases are considered
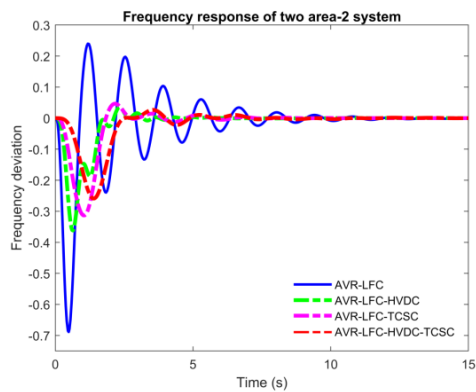
Figure 17. Frequency Deviation of area-2 For MAMS-IPC, PSO-PID all four cases are considered
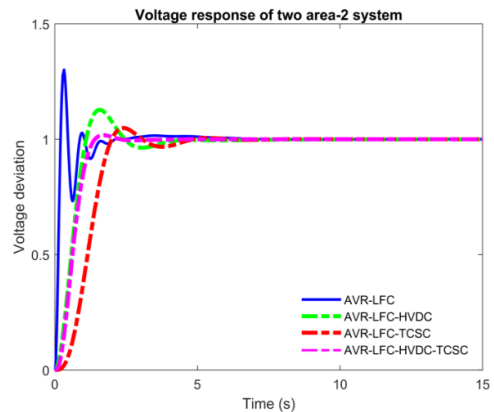
Figure 20. Voltage Deviation of area-2 For MAMS-IPC, PSO-PID all four cases are considered
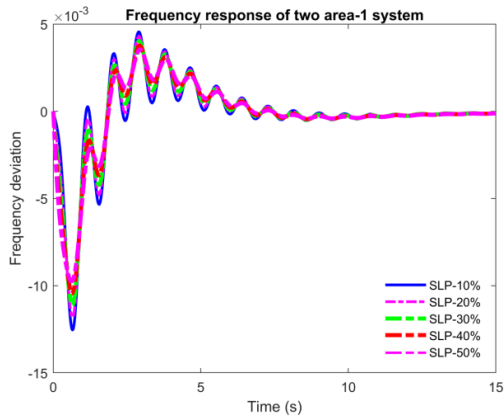
Figure 21. Frequency Response at Different loading conditions for area-1, Proposed PI-PD controller is implemented for case-04
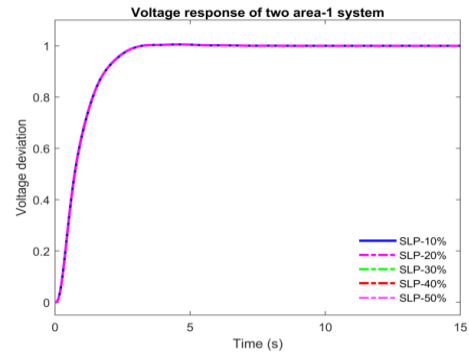
Figure 24. Voltage Response at Different loading condition for area-1, Proposed PI-PD controller is implemented for case-04
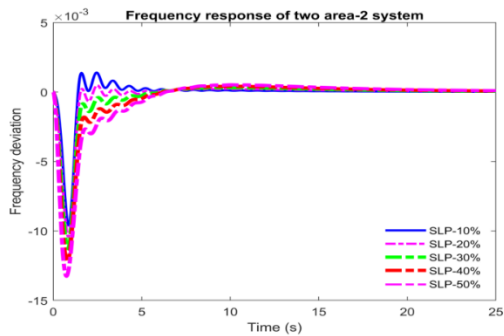
Figure 22. Frequency Response at Different loading conditions for area-2, Proposed PI-PD controller is implemented for case-04
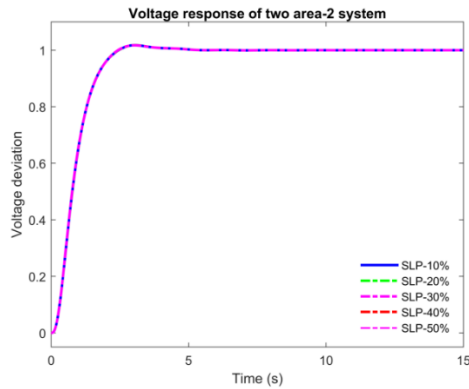
Figure 25.Voltage Response at Different loading condition for area-2, Proposed PI-PD controller is implemented for case-04
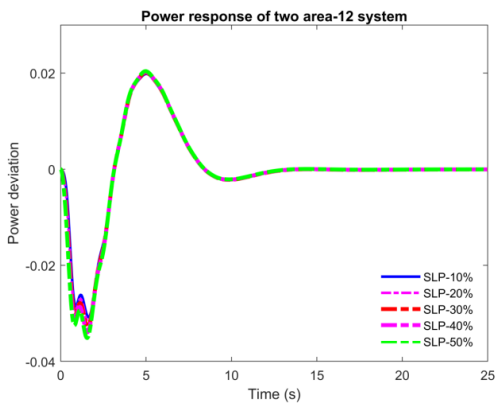
Figure 23. Power Response at Different Loading condition for area-12, Proposed PI-PD controller is implemented for case-04
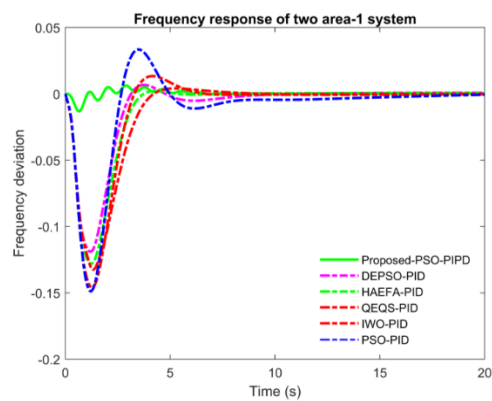
Figure 26. Frequency response of area-1, Proposed PI-PD controller is implemented for case-04[19, 21-23, 27]
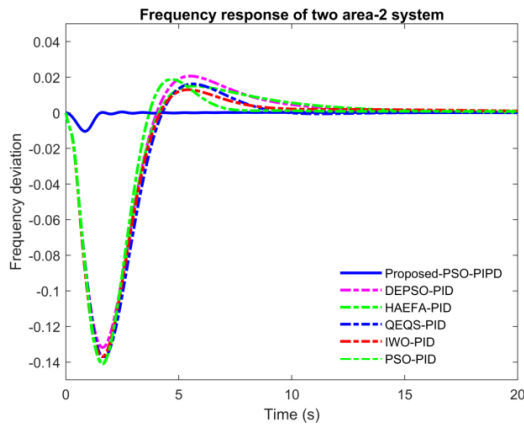
Figure 27. Frequency response of area-2, Proposed PI-PD controller is implemented for case-04[19, 21-23, 27]
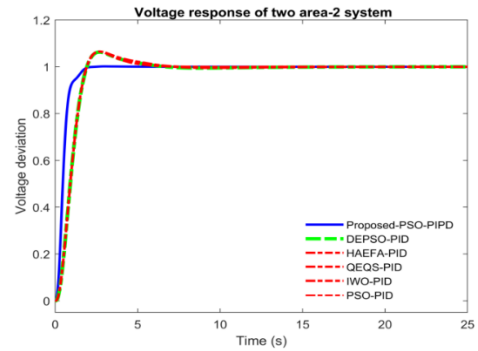
Figure 30. Voltage response of area-2, Proposed PI-PD controller is implemented for case-04[19, 21-23, 27]
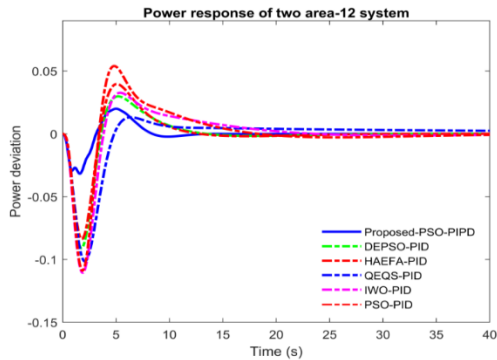
Figure 28. Frequency response of area-2, Proposed PI-PD controller is implemented for case-04 [19, 21-23, 27]
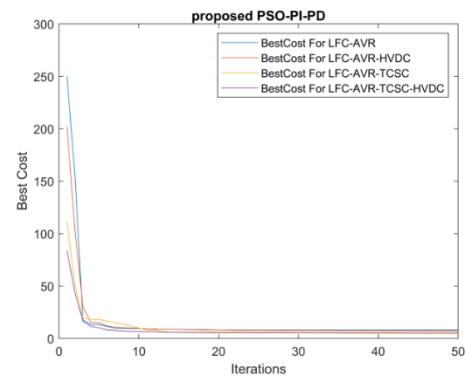
Figure 31. Iteration graph for Different cases obtained by PSO-PI-PD controller
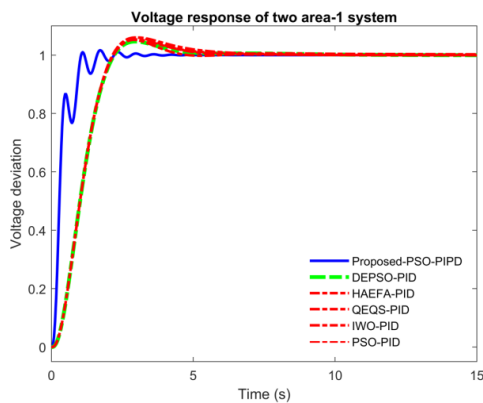
Figure 29. Voltage response of area-1, Proposed PI-PD controller is implemented for case-04[19, 21-23, 27]
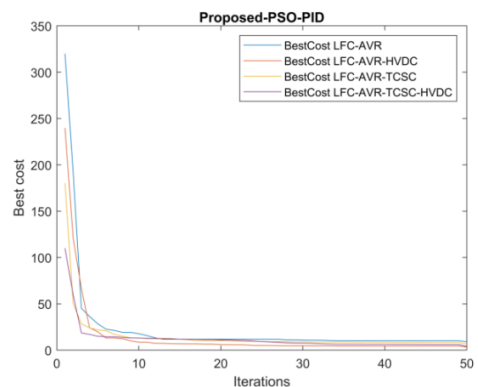
Figure 32. Iteration graph for Different cases obtained by PSO-PID controller

Table 3. Results obtained By Proposed PSO-PI-PD, based on Settling-Time cases are compared

S.NO	Different Cases	Δf_1	Δf_2	ΔP_{12}	Δv_1	Δv_2
1	Case-01	7.1525	7.0347	12.0653	3.91814	3.45561
2	Case-02	4.9309	6.80152	3.68492	2.42022	2.50891
3	Case-03	5.3852	4.21513	8.80854	1.70591	1.72964
4	case-04	2.2198	2.36002	2.69232	1.03661	1.62710

Table 4. Results obtained By Proposed PSO-PI-PD, based on Peak-Time cases are compared

S.NO	Different Cases	Δf_1	Δf_2	ΔP_{12}	Δv_1	Δv_2
1	Case-01	0.11330	0.06507	0.1334063	1.070574	1.21889
2	Case-02	0.059572	0.03772	0.040278	1.05340	1.1256426
3	Case-03	0.02879598	0.021270	0.034141493	1.0359785	1.1219219
4	Case-04	0.01208870	0.03102455	0.011920715	0.9151454	1.0694207

Table.5 Comparison of all cases based on Performance indices Proposed PSO-PI-PD

S.no	Different cases	ITAE	ITSE	IAE	ISE
1	Case-01	3.0090	0.7696	2.7273	1.5430
2	Case-02	2.1006	0.7335	2.6828	1.5198
3	Case-03	2.5784	0.6396	2.3349	1.3123
4	Case-04	0.9087	0.2428	1.5624	0.7708

Table 6. Results obtained By Proposed PSO-PID, based on Settling-Time cases are compared

S.NO	Different Cases	Δf_1	Δf_2	ΔP_{12}	Δv_1	Δv_2
1	Case-01	8.626438564	8.7856906	14.876410	3.1152061	2.500701
2	Case-02	3.853160	3.3839599	4.2610885	1.6532283	2.296909
3	Case-03	2.69890658	2.75762206	3.939177	1.4843511	1.9989065
4	Case-04	2.412496013	2.644903257	3.7075930	1.2458474	1.1070281

Table.7 Results obtained By Proposed PSO-PID, based on Peak-Time cases, are compared

S.NO	Different Cases	Δf_1	Δf_2	ΔP_{12}	Δv_1	Δv_2
1	Case-01	0.10765540	0.286746492	0.1006690	1.2556577	1.325206
2	Case-02	0.093533494	0.050553489	0.06651458	1.24236738	1.257753
3	Case-03	0.06923781	0.031525112	0.0494577	0.99730737	1.187922
4	Case-04	0.026864	0.0153950	0.0361161	0.8380071	1.069420

Table.8 Comparison of all cases based on Performance indices Proposed PSO-PID

S.no	cases	ITAE	ITSE	IAE	ISE
1	Case-01	6.0068	0.5538	4.6913	0.9214
2	Case-02	3.7036	0.2563	3.7720	0.7113
3	Case-03	2.4970	0.2107	2.8066	0.5079
4	Case-04	1.6382	0.1946	1.4473	0.3078

6. CONCLUSION

In this paper, MAMS-IPS, incorporated with AVR, is considered for the LFC study. This work is divided into four different cases. Conventional PID and hybrid PI-PD controllers are proposed for minimizing the steady error. The suggested controller values are optimized using a nature-inspired method based on particle swarm optimization (PSO). The robustness of the suggested controller implemented for MAMS-IPS is verified by applying different loading conditions. A step load of 10% is applied to both areas. To assess the superiority of the suggested controller, its response results are compared with those of a PID controller tuned from recently published literature on novel algorithms. A comparison of the results based on setting time, peak time, and rise time is conducted. The results obtained by the proposed PI-PD controller are better than those obtained by the conventional controller. The effect of the HVDC Link and FACT Device is also observed, and its results are compared with the base model (LFC-AVR) results. Comparisons of different cases are done based on performance indices such as ISE, ITAE, ITSE, and IAE, and also by assessing the settling time and peak time of the response. The LFC-AVR-HVDC-TCSC shows better results compared to other cases. Eigenvalue analysis is also conducted for all the different proposed models to test their stability. In the future, this work can be extended by applying renewable energy sources in each area and assessing their effects. Additionally, energy storage devices can also be incorporated with conventional energy sources, and their effects can be absorbed.

Table.9 Comparison of Proposed (PI-PD-PSO) controller demonstrated for LFC-AVR-HVDC-TCSC (case-04) based on Settling-Time from Recent literature

S.No	Parameters of system	Proposed PI-PD controller for (AVR-AGC-TCSC-HVDC)	DEPSO-PID[22]	HAEFA-PID[19]	QEQS-PID[21]	IWO-PID[23]	PSO-PID[27]
1	ΔF_1	2.512496013027371	15.4321	8.0767	3.5399	6.5727	5.7901
2	ΔF_2	2.744903257853773	6.8770	11.6899	12.2194	8.5671	9.1088
3	ΔP_{12}	3.877593080806343	17.0709	19.7859	11.9922	15.5245	21.0371
4	ΔV_1	1.645847495463177	3.9554	4.1550	4.5187	4.9780	4.4967

| 5 | ΔV_2 | 1.977028140290292 | 4.4666 | 4.7410 | 4.8725 | 5.1479 | 4.9337 |

Table 10.Comparison of Proposed (PI-PD-PSO) controllers demonstrated for LFC-AVR-HVDC-TCSC (case-04) based on Rise-Time from Recent literature

S.No	Parameters of system	Proposed PI-PD controller for (AVR-AGC-TCSC-HVDC)	DEPSO-PID[22]	HAEFA-PID[19]	QEQS-PID[21]	IWO-PID[23]	PSO-PID[27]
1	ΔF_1	0.00008621382	0.0048	0.0054	0.0105	0.0006606	0.0036
2	ΔF_2	0.00008422145147	0.0060	0.0036	0.0035	0.0013	0.0001406
3	ΔP_{12}	0.00000113507	0.1195	0.00030	0.0009198	0.0984	0.1090
4	ΔV_1	0.78088284913985	1.3614	1.3815	1.3743	1.3734	1.3623

Table 11. Eigenvalues for different Cases obtained by PI-PD-PSO optimization technique

S.NO	AGC-AVR	AGC-AVR-HVDC	AGC-AVR-TCSC	AGC-AVR-TCSC-HVDC
1	-3.3333 + 0.0000i	-3.3333 + 0.0000i	-3.3333 + 0.0000i	-0.73405 + 0.0000i
2	-3.3333 + 0.0000i	-3.3333 + 0.0000i	-3.3333 + 0.0000i	-3.3333 + 0.0000i
3	-0.1000 + 0.0000i	-0.1000 + 0.0000i	-0.1000 + 0.0000i	-3.3333 + 0.0000i
4	-0.1000 + 0.0000i	-0.1000 + 0.0000i	-0.1000 + 0.0000i	-0.1000 + 0.0000i
5	-80.0549 + 0.00000i	-80.0469 + 0.0186i	-80.04054 + 0.0000i	-0.1000 + 0.0000i
6	-80.0321 + 0.00000i	-80.0469 - 0.0186i	-80.0496 + 0.00i	-80.048 + 0.02231i
7	-19.482 + 0.00i	-18.8415 + 0.000i	-19.474 + 0.000i	-80.048 - 0.02231i
8	-19.851 + 0.013403i	-19.95251 + 0.08595i	-19.8521 + 0.00i	-19.915 + 0.14781i
9	-19.8510- 0.0134i	-19.95321 - 0.0859i	-19.8379 + 0.00i	-19.9152 - 0.14781i
10	-19.371 + 0.000000i	-19.6487 + 0.00000i	-19.3254 + 0.000i	-17.1013 + 3.296i
11	-11.794 + 0.0000i	-13.3070 + 0.00000i	-11.809 + 0.00000i	-17.1016 - 3.29640i
12	-12.07929 + 0.000i	-1.1213 + 7.52328i	-12.209 + 0.0000i	-18.6921 + 0.00000i
13	-7.13698+ 0.345118i	-1.121344 - 7.5232i	-12.5000 + 0.000i	-1.5695 + 7.64767i
14	-7.1368 - 0.34511i	-11.3276 + 0.0000i	-12.500 + 0.000i	-1.56957 - 7.64767i
15	-12.5000 + 0.0000i	-12.5000 + 0.0000i	-7.2774 + 0.00000i	-13.5673 + 0.0000i
16	-12.500+ 0.00000i	-12.50000 + 0.000i	-7.032 + 0.000000i	0.763001 + 5.3264i
17	-0.37923 + 4.42i	-5.1507 + 3.376539i	-0.4419 + 4.66893i	0.76901 - 5.326449i
18	-0.3462 - 4.42572i	-5.157 - 3.37599i	-0.4452219 - 4.6693i	-12.50 + 0.00000i
19	-0.28661 + 3.70345i	-6.2187 + 0.00000i	-0.181906 + 3.54589i	-12.5 + 0.0000i
20	-0.28661 - 3.70345i	-0.103664 + 3.61076i	-0.186806 - 3.54419i	-6.4202 + 1.60490i
21	-0.28280 + 2.73803i	-0.103464 - 3.6176i	-0.21061 + 2.94832i	-6.42102 - 1.60490i
22	-0.256280 - 2.7383i	-0.58064 + 3.64580i	-0.21061 - 2.94832i	-0.4053 + 4.09010i
23	-0.45188 + 2.6253i	-0.58764 - 3.64590i	-0.3215 + 2.5701i	-0.42953 - 4.09040i
24	-0.456288 - 2.623i	-0.76904 + 2.14118i	-0.379815 - 2.5701i	-0.0863 + 3.41856i
25	-3.135 + 0.021709i	-0.7604 - 2.147618i	-3.15956 + 0.0000i	-0.08663 - 3.41i
26	-3.165 - 0.02169i	-3.38841 + 0.000i	-3.1961 + 0.000i	-2.3963 + 1.8421i
27	-2.1843 + 0.16908i	-3.0923 + 0.0000i	-2.4121505 + 0.000i	-2.39123 - 1.88021i
28	-2.143 - 0.1698i	-2.84446 + 0.000i	-1.931 + 0.0000i	-3.1112 + 0.046926i
29	-1.05328 + 0.0000i	-1.3587 + 0.0000i	-0.226 + 0.732i	-3.1112 - 0.046926i
30	-0.86325 + 0.028i	-1.04117 + 0.000i	-0.2596 - 0.738972i	-1.51000 + 0.38553i
31	-0.8985 - 0.021438i	-0.67550 + 0.000i	-1.2282 + 0.0000i	-1.510 - 0.39553i
32	-0.15878 + 0.38298i	-1.4478167 + 0.000i	-1.019376 + 0.000i	-0.838543 + 00000i
33	-0.1158 - 0.3798i	-1.4463 + 0.0000i	-0.86154 + 0.00000i	-0.663680 + 0.000i
34	-1.44667 + 0.00i	-0.50786 + 0.000i	-0.93008 + 0.000i	-0.51121 + 0.000i
35	-1.48167 + 0.00i	-0.31686 + 0.0000i	-1.446967 + 0.0000i	-0.37916 + 0.00000i
36	-0.0695 + 0.000i	-0.22321 + 0.0000i	-1.44667 + 0.00000i	-1.017167 + 0.0000i
37	-0.0377 + 0.000i	-0.06245 + 0.0000i	-0.06170 + 0.0000i	-1.446167 + 0.0000i
38	-0.09921+ 0.000i	-0.0351 + 0.000000i	-0.034739 + 0.0000i	-0.060493+ 0.0000i
39	-0.091 + 0.00i	-0.099 + 0.000i	-0.09921 + 0.000i	-0.0349 + 0.0000i
40	-0.0035 + 0.013i	-0.09921 + 0.000i	-0.099 + 0.0000i	1.176e-14 + 0.0000i
41	-0.0324- 0.0103i	-0.00247 + 0.01130i	-0.00347 + 0.01130i	-1.706e-15 + 0.000i
44	-0.032 + 0.0303i	-0.0047 - 0.011303i	-0.00352479 - 0.011i	-0.003279 + 0.0113i
43	-0.0047 - 0.0113i	-0.003524 + 0.011i	-0.00352 + 0.011i	-0.00352 - 0.0113i
44	2.01e-14 + 0.00i	-0.003524 - 0.0103i	-0.00247 - 0.01130i	-0.00327 + 0.01130i
45	-2.13e-17 + 0.0i	-3.17e-14 + 0.0000i	-2.222e-14 + 0.0000i	-0.0035279 - 0.011i
46	0.0000 + 0.0000i	-5.6590e-15 + 0.0i	1.515e-15 + 0.0000i	-0.099214 + 0.000i
47	0.0000 + 0.0000i	0.0000 + 0.0000i	0.0000 + 0.0000i	-0.0992175+ 0.00i

REFERENCES

[1]   A. Nayak., M. K. Maharana., *Performance Assessment of Fuzzy Logic Controller for Load Frequency Control in multi source multi area system*, International Journal of Renewable Energy Research (IJRER), vol. 9, no. 4, pp. 1597-1605 (2019), DOI: 10.20508/ijrer.v9i4.9758.g7762.

[2]   M. A. R. Shafei., A. N. Abd Alzaher., D. K. Ibrahim., *Enhancing load frequency control of multi-area multi-sources power system with renewable units and including nonlinearities*, Indonesian Journal of Electrical Engineering and Computer Science, vol. 19, no. 1, pp. 108-118 (2020), DOI: 10.11591/ijeecs.v19.i1.pp108-118.

[3]   A. Kumar., S. Suhag., *Effect of TCPS, SMES, and DFIG on load frequency control of a multi-area multi-source power system using multi-verse optimized fuzzy-PID controller with derivative filter*, Journal of Vibration and Control, vol. 24, no. 24, pp. 5922-5937 (2018), DOI:10.1177/1077546317724968.

[4]   D. K. Lal., A. Barisal., *Comparative performances evaluation of FACTS devices on AGC with diverse sources of energy generation and SMES*, Cogent Engineering, vol. 4, no. 1, p. 1318466 (2017), DOI: 10.1080/23311916.2017.1318466

[5]   K. Jagatheesan., B. Anand., S. Samanta., N. Dey., A. S. Ashour., V. E. Balas., *Particle swarm optimisation-based parameters optimisation of PID controller for load frequency control of multi-area reheat thermal power systems*, International Journal of Advanced Intelligence Paradigms, vol. 9, no. 5-6, pp. 464-489 (2017), DOI:10.1504/IJAIP.2017.088143.

[6]   R. Choudhary., J. Rai., Y. Arya., *Automatic generation control for single area power system using GNA tuned PID controller*, in Journal of Physics: Conference Series, (2020), vol. 1478, no. 1: IOP Publishing, p. 012011, DOI:10.1088/1742-6596/1478/1/012011.

[7]   B. Mohanty., S. Panda., P. Hota., *Controller parameters tuning of differential evolution algorithm and its application to load frequency control of multi-source power system*, International journal of electrical power & energy systems, vol. 54, pp. 77-85 (2014), DOI: 10.1016/j.ijepes.2013.06.029.

[8]   A. Panwar., G. Sharma., R. C. Bansal., *Optimal AGC design for a hybrid power system using hybrid bacteria foraging optimization algorithm*, Electric Power Components and Systems, vol. 47, no. 11-12, pp. 955-965 (2019), DOI: 10.1080/15325008.2019.1659452.

[9]   M. Deepak., R. J. Abraham., *Load following in a deregulated power system with thyristor controlled series compensator*, International Journal of Electrical Power & Energy Systems, vol. 65, pp. 136-145 (2015), DOI: 10.1016/j.ijepes.2014.09.038.

[10]   J. Morsali., K. Zare., M. T. Hagh., *Performance comparison of TCSC with TCPS and SSSC controllers in AGC of realistic interconnected multi-source power system*, Ain shams engineering journal, vol. 7, no. 1, pp. 143-158 (2016), DOI:10.1016/j.asej.2015.11.012.

[11]   V. Nath., D. Sambariya., *Analysis of AGC and AVR for single area and double area power system using fuzzy logic control*, International Journal of Advanced Research in Electrical, Electronics and Instrumentation Engineering, vol. 4, no. 7, pp. 6501-6511 (2015), DOI: 10.15662/ijareeie.2015.0407075.

[12]   V. Nath., D. K. Sambariya., *Design and performance analysis of adaptive neuro fuzzy controller for load frequency control of multi-power system*, International Conference on Intelligent Systems and Control (ISCO), pp. 1-7(2016), DOI: 10.1109/ISCO.2016.7726986.

[13]   D. Sambariya and V. Nath, *Optimal control of automatic generation with automatic voltage regulator using particle swarm optimization*, Universal Journal of Control and Automation, vol. 3, no. 4, pp. 63-71 (2015), DOI: 10.13189/ujca.2015.030401

[14]   D. Sambariya.,V. Nath., *Load frequency control using fuzzy logic based controller for multi-area power system*," British Journal of Mathematics & Computer Science, vol. 13, no. 5, pp. 1-19(2016), DOI: 10.9734/BJMCS/2016/22899.

[15]   D. K. Sambariya., V. Nath., *Application of NARMA L2 controller for load frequency control of multi-area power system*, in 2016 10th International Conference on Intelligent Systems and Control (ISCO), 7-8 Jan, pp. 1-7(2016), DOI: 10.1109/ISCO.2016.7726987.

[16]   G. Sharma., I. Nasiruddin., K. R. Niazi., R. C. Bansal., *Robust automatic generation control regulators for a two-area power system interconnected via AC/DC tie-lines considering new structures of matrix Q*, IET Generation, Transmission & Distribution, vol. 10, no. 14, pp. 3570-3579, 2016.

[17]   Y. Arya., N. Kumar., *AGC of a multi-area multi-source hydrothermal power system interconnected via AC/DC parallel links under deregulated environment*, International Journal of Electrical Power & Energy Systems, vol. 75, pp. 127-138 (2016), DOI: 10.1016/j.ijepes.2015.08.015.

[18]   E. Rakhshani., K. Rouzbehi., M. A. Elsaharty., P. R. Cortes., *Heuristic optimization of supplementary controller for VSC-HVDC/AC interconnected grids considering PLL*, Electric Power Components and Systems, vol. 45, no. 3, pp. 288-301 (2017), DOI: 10.1080/15325008.2016.1232765.

[19]   C. Kalyan., G. S. Rao., *Coordinated SMES and TCSC Damping Controller for Load Frequency Control of Multi Area Power System with Diverse Sources*, International Journal on Electrical Engineering & Informatics, vol. 12, no. 4, (2020), DOI: 15676/ijeei.2020.12.4.4.

[20] R. K. Khadanga., A. Kumar., *Analysis of PID controller for the load frequency control of static synchronous series compensator and capacitive energy storage source-based multi-area multi-source interconnected power system with HVDC link*, International Journal of Bio-Inspired Computation, vol. 13, no. 2, pp. 131-139 (2019), DOI: 10.1504/IJBIC.2019.098413.

[21] Vigya., C. K. Shiva., B. Vedik., V. Mukherjee., *Comparative analysis of PID and fractional order PID controllers in automatic generation control process with coordinated control of TCSC*, Energy Systems, vol. 14, no. 1, pp. 133-170 (2023), DOI: 10.1007/s12667-021-00457-5.

[22] D. K. Lal., A. K. Barisal., M. Tripathy., *Load frequency control of Multi Source Multi-Area nonlinear power system with De-pso Optimized Fuzzy pid controller in coordination With SSSC and RFB*, Int. J. Control. Autom, vol. 11, pp. 61-80, (2018), DOI: 10.14257/ijca.2018.11.7.06.

[23] S. Mishra., A. K. Barisal., B. C. Babu., *Invasive weed optimization-based automatic generation control for multi-area power systems*, International Journal of Modelling and Simulation, vol. 39, no. 3, pp. 190-202 (2019), DOI: 10.1080/02286203.2018.1554403.

[24] G. Paliwal., K. Parkh., R. Jangid., *Load Frequency Control of Multi-Area MultiSource Power System by Gray Wolf Optimization Technique*, International Journal of Research in Engineering, Science and Management vol. 2, no. 2, (2020).

[25] K. Challapalli., B. Goud., M. Bajaj., M. Kumar., E. Ahmed., S. Kamel., *Water-Cycle-Algorithm-Tuned Intelligent Fuzzy Controller for Stability of Multi-Area Multi-Fuel Power System with Time Delays*," p. 508, (2022), DOI: 10.3390/math10030508.

[26] N. S. Kalyan., G. Sambasiva Rao., *Frequency and voltage stabilisation in combined load frequency control and automatic voltage regulation of multiarea system with hybrid generation utilities by AC/DC links*, International Journal of sustainable energy, vol. 39, no. 10, pp. 1009-1029 (2020), DOI: 10.1080/14786451.2020.1797740.

[27] C. N. S. Kalyan *et al.*, *Comparative performance assessment of different energy storage devices in combined LFC and AVR analysis of multi-area power system*, Energies, vol. 15, no. 2, p. 629, (2022), DOI: 10.3390/en15020629.

[28] D. Guha., P. K. Roy., S. Banerjee., *Application of backtracking search algorithm in load frequency control of multi-area interconnected power system*, Ain Shams Engineering Journal, vol. 9, no. 2, pp. 257-276 (2018), DOI: 10.1016/j.asej.2016.01.004.

[29] D. Guha., P. K. Roy., and S. Banerjee., *Symbiotic organism search algorithm applied to load frequency control of multi-area power system*, Energy Systems, vol. 9, pp. 439-468, 2018, DOI: 10.1007/s12667-017-0232-1.

[30] A. Daraz., S. A. Malik., H. Mokhlis., I. U. Haq., G. F. Laghari., N. N. Mansor., F*itness dependent optimizer-based automatic generation control of multi-source interconnected power system with non-linearities*, Ieee Access, vol. 8, pp. 100989-101003 (2020), DOI: 10.1109/ACCESS.2020.2998127.

[31] S. Tripathy., R. Balasubramanian., P. Nair., *Effect of superconducting magnetic energy storage on automatic generation control considering governor deadband and boiler dynamics*, IEEE Transactions on Power systems, vol. 7, no. 3, pp. 1266-1273 (1992), DOI: 10.1109/59.207343.

[32] H. Li., *Tuning of PI–PD controller using extended non-minimal state space model predictive control for the stabilized gasoline vapor pressure in a stabilized tower*, Chemometrics and Intelligent Laboratory Systems, vol. 142, pp. 1-8, (2015), DOI: 10.1016/j.chemolab.2014.12.012.

[33] T. Ali., S. A. Malik., I. A. Hameed., A. Daraz., H. Mujlid., A. T. Azar., *Load frequency control and automatic voltage regulation in a multi-area interconnected power system using nature-inspired computation-based control methodology*, Sustainability, vol. 14, no. 19, p. 12162, (2022).

[34] I. Kaya., *Optimal PI–PD controller design for pure integrating processes with time delay*, Journal of Control, Automation and Electrical Systems, vol. 32, no. 3, pp. 563-572, 2021, DOI: 10.1007/s40313-021-00692-2.

[35] G. Lloyds Raja., A. Ali., *New PI-PD controller design strategy for industrial unstable and integrating processes with dead time and inverse response*, Journal of Control, Automation and Electrical Systems, vol. 32, pp. 266-280 (2021), DOI: 10.1007/s40313-020-00679-5.

[36] N. V. Kumar., M. M. T. Ansari., *A new design of dual mode Type-II fuzzy logic load frequency controller for interconnected power systems with parallel AC–DC tie-lines and capacitor energy storage unit*, International Journal of Electrical Power & Energy Systems, vol. 82, pp. 579-598, (2016), DOI: 10.1016/j.ijepes.2016.03.063.

[37] A. Khanjanzadeh., S. Soleymani., B. Mozafari., M. Fotuhi., *Integrated multi-area power system with HVDC tie-line to enhance load frequency control and automatic generation control*, Electrical Engineering, vol. 102, pp. 1223-1239 (2020), DOI: 10.1007/s00202-020-00944-5.

[38] V. Dhawane., D. Bichkar., *Load frequency control optimization using PSO based integral controller*, International Journal of Recent Technology and Engineering (IJRTE), vol. 8, no. 6, pp. 97-103 (2020), DOI: 10.35940/ijrte.E6749.038620.

[39] A. M. A. Soliman., M. Bahaa., M. A. Mehanna., *PSO tuned interval type-2 fuzzy logic for load frequency control of two-area multi-source interconnected power system*, Scientific Reports, vol. 13, no. 1, p. 8724 (2023), DOI: 10.1038/s41598-023-35454-4.

[40] B. Dhanasekaran., J. Kaliannan., A. Baskaran., N. Dey., J. M. R. Tavares., *Load Frequency Control Assessment of a PSO-PID Controller for a Standalone Multi-Source Power System*, Technologies, vol. 11, no. 1, p. 22 (2023), DOI: 10.3390/technologies11010022.

BIOGRAPHY OF AUTHORS

Vivek Nath was born in July 1992. He received the B.Tech. degree in Electrical & Electronics Engineering from Vyas Institute of Engineering & Technology, Jodhpur, India in 2012. Currently, he is pursuing Phd degree from the Department of Electrical Engineering, Rajasthan Technical University, Kota, 324010, Rajasthan, India. His interest is in wide - area power system and control including load frequency control (LFC), HVDC and FACTS Devices in power systems

D. K. Sambariya was born in Heerapur, Bharatpur (Raj.), India on December 10, 1971. He graduated from the Malaviya Regional Engineering College (MREC) currently known as Malaviya National Institute of Technology (MNIT), Jaipur. He have completed post graduation from University of Rajasthan (UOR) and completed Ph. D. from Department of Electrical Engineering, Indian Institute of Technology Roorkee, Roorkee, India. His employment experience included the Department of Electrical Engineering, Engineering College, Kota since 1996 as Lecturer. He is currently serving at Department of Electrical Engg., Rajasthan Technical University, Kota, 324010, India, as Associate Professor. His research interests include applications fuzzy logic, soft computing techniques and classical control techniques in the field of power system. He is also involved in the reduction of large scale systems to its lower order model with retention of the properties of the original system.